Eleventh International Conference on Computational Fluid Dynamics (ICCFD11), Maui, HI, July 11-15, 2022 **ICCFD11-2022-3005**

Development of Three-Dimensional Ray Tracing Solver for Communication Blackout in Atmospheric Entries

Vincent F. Giangaspero*,**, V. Sharma*, S. Poedts*,*** and A.Lani*,**
Corresponding author: vincent.giangaspero@kuleuven.be

* Center for Mathematical Plasma-Astrophysics, KU Leuven, Belgium
** Aeronautics and Aerospace Department, von Karman Institute for Fluid Dynamics, Belgium
*** Institute of Physics, University of Maria Curie-Skłodowska, Poland

06/24/2022

Abstract:
This works presents the development of a three-dimensional solver for the numerical analysis of the communication blackout encountered in atmospheric entry flights. The proposed methodology is based on computational fluid dynamic (CFD) simulation in combination with a ray tracing numerical technique. The ray tracing algorithm is based on the implementation of the Eikonal system of equation, a fast, efficient and accurate method to analyse interaction of electromagnetic signals and weakly ionised plasmas. The proposed methodology is applied to the atmospheric entry of the ExoMars capsule in Martian environemnt and shows the capability of a three-dimensional approach to analyse real flight configuration. Results demonstrate the validity of the proposed ray tracing approach for the analysis of communication blackout, where signals emitted from the on-board antenna undergo reflection and refraction from the plasma surrounding the entry vehicle.

Keywords: Numerical Algorithms, Computational Fluid Dynamics, Plasma flows, Hypersonics, Communicaition Blackout

1 Introduction

The re-entry phase is one of the most challenging phases of a space mission and it's one of the most critical aspects to be considered for the design of a successful space mission. Spacecraft flying at hypersonic speeds undergo large pressure and thermal loads, which, if not properly quantified, may compromise structural integrity and result in mission failure [1]. Furthermore, communication systems are disrupted during this delicate phase, ultimately compromising data transmission and control [2]. Since the early days of the space era, communication blackout has been an open challenge and no active solutions have been developed so far. Developing strategies to ensure propagation of radio signals from/to ground control is of paramount importance for the success of a space mission. The reduction of the overall communication blackout period would limit data transmission losses and therefore lead to safer control during entry. This is one of the key challenges for the future of the aerospace sector, for future human space flights, space tourism or military applications that will all require telecommunications improvements during flight at hypersonic speeds.

The methodology proposed in this work is focused on the innovative use of optical ray tracing to characterize the phenomena of the communications blackout. This will allow to overcome the limits of the current state-of-the-art approaches that are not capable to deliver the information needed to develop blackout mitigation solutions for future space missions. This paper presents the development of a three dimensional ray tracing solver to analyse communication blackout. The solver needs vehicle geometry, antenna characteristics and location, and the plasma distribution around a spacecraft computed by non-equilibrium hypersonic simulations as input. The propagation of the electromagnetic (EM) waves radiated by the on board antenna through the plasma is modeled using a ray tracing "shooting-and-bouncing" technique through the non-uniform plasma region around the vehicle until it escapes from the plasma region. The case study analysed in this work is the entry of the 2016 ESA ExoMars mission lander, which experienced $60s$ of blackout [3]. This mission consisted in the launch of the ExoMars Trace Gas Orbiter (TGO), an atmospheric research orbiter, and the deployment of Schiaparelli, the Entry, Descent, and Landing Demonstrator Module (EDM). The objective of the landing mission was to assess and validate ESA's technologies capabilities in preparation of future missions [4]. Bi-dimensional axi-symmetric hypersonic CFD simulations are performed over the ExoMars Schiaparelli module at three different trajectory points with the COOLFluiD aerothermodynamics Finite Volume solver coupled with the thermochemistry library PLATO. The axi-symmetric CFD solutions are then extruded and rotated to generate a three-dimensional flow solution, that is used as an input from the ray tracing three-dimensional solver. The ray tracing algorithm is implemented in the Matlab software code Black-Out-RAy-Tracer (BORAT), of which version 3.0 has been developed for its three-dimensional version.

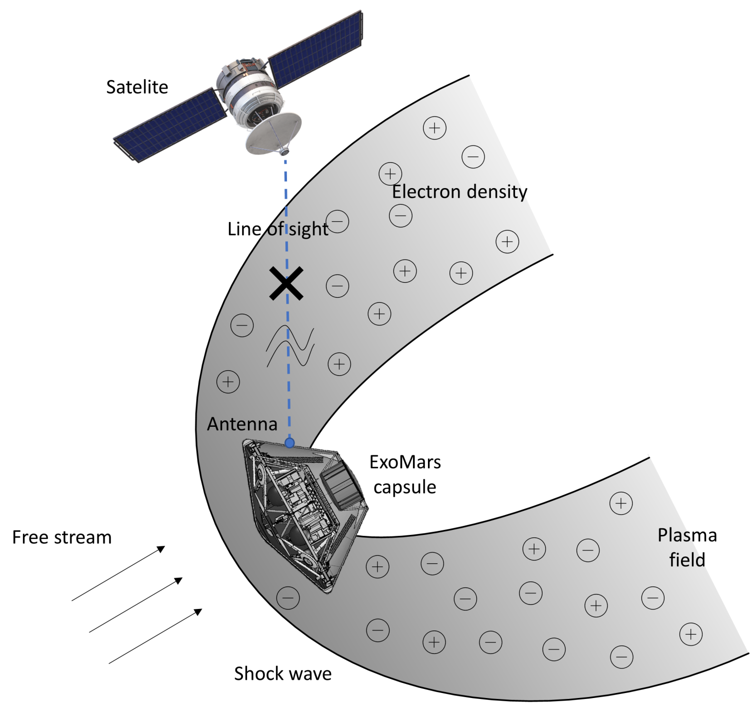

Figure 1: Radio frequency blackout for flow over entry capsule.

2 Communication Blackout

During the entry phase, spacecraft enter a planetary atmosphere at hypersonic speed, typically around 6-10 $km\ s^{-1}$, generating strong shock waves and large aerodynamic heating [5]. When the temperature is high enough to excite the gas molecule internal energy modes up to the point where dissociation and ionization reactions occur, a plasma layer is generated around the vehicle. Plasma interacts with the electromagnetic fields signals from/to the vehicle, disrupting the functionality of the on-board signal transmission systems [6]. The created plasma layer usually has an electron number density of 10^{17} to 10^{20} m^{-3} [7]. The amount of electrons generated in the plasma field characterizes the ionization level of the plasma, that in communication problems is quantified by the plasma natural resonant frequency. For a given electron number density N_e, the plasma frequency has a square root dependence on the electron number density $f_p \sim \sqrt{N_e}$. Plasma attenuates the radio frequency (RF) signal used for communication when the transmission frequency is comparable to the plasma frequency [8]. At each transmission frequency corresponds a plasma flow critical electron density $N_{e_{crit}}$ that, if generated in the re-entry plasma layer, results in blackout conditions. Figure 1 shows a sketch representation of the radio communication blackout for a re-entry capsule. At the beginning of an entry flight, electron production is generally low due to the low density of the atmosphere. As the capsule flies at higher-speed through denser atmospheric layers, electron production increases, reaching a maximum approximately at the peak of aerodynamic heating. After this phase, the electron production diminishes due to the lower speed of the capsule during the final landing phase. In general higher ionisation levels occur in the front part of the vehicle, in the proximity of the stagnation zone. For this reason, entry capsules usually place their antenna in the backshell of the vehicle. However, at the peak of communication blackout, the plasma region propagates considerably in the wake, disrupting the signal propagation also in this region [9].

3 Radio-blackout analysis methodology

Numerical analysis of communication blackout during re-entry involves two different steps:

- Obtain electron density profiles from Computational Fluid Dynamics (CFD) simulations.
- Predict electromagnetic wave propagation through plasma.

Different electromagnetic wave propagation models have been proposed in the literature including the plasma frequency approach [10, 11], geometrical optics, ray tracing [12, 13] and using a finite difference scheme to solve the Maxwell equations directly [14]. For Mars entry missions, very limited work has been published, where the Line Of Sight (LOS) approach was used to verify the results [11]. This simple technique is based on the comparison between the maximum and critical electron number density along the LOS between the spacecraft and the receiving satellite. The main limitation of this approach is the lack of multidimensional information on the interaction between the RF signal and the plasma. Moreover, the use of highly advanced methods allows for reproducing more complex waves phenomena such as reflection, refraction and phase modulation. Ray based techniques are advanced methods widely applied to ionosphere communication, and intrinsically well suited to analyse electrically large problems. Ramjatan [12] proposed the first but a very primitive application of ray tracing to the Martian entry and has been the first study in literature of the ExoMars Schiaparelli blackout period employing a decoupled CFD approach along with a simple ray tracing algorithm. The present work describes a significantly more refined model and presents major upgrades with respect to the original method proposition. Some of the advantages of the upgraded methodology have been reported in [13]. The present work focuses on the development of an advanced and much more accurate ray tracing algorithm, based on the high frequency Eikonal approximation, which is more accurate and suitable in predicting the propagation of EM waves within the plasma region, especially for three-dimensional cases and real flight conditions.

3.1 CFD plasma model

The hypersonic flow generated around the entry vehicle is computed by solving the Navier-Stokes equations. The flow is described as a single-fluid accounting for chemical non-equilibrium effects. The numerical simulations are performed with the aerothermodynamic solver implemented in the COOLFluiD platform [15, 16]. This solver is a parallel unstructured 2-D/3-D cell-centered finite volume solver tool of simulating hypersonic chemically reacting and plasma [17, 18]. The numerical convective flux is computed with the AUSUM+ scheme [19]. Second-order accurate solutions are obtained by means of a weighted linear least square reconstruction [20], relying on the Venkatakrishnan limiter [21] for removing spurious oscillations around shocks.

Plasma thermodynamic and transport properties, along with source terms due to the kinetic processes (*e.g.*, dissociation), are computed using the PLATO (PLAsmas in Thermodynamic nOn-equilibrium) library, which has been coupled to COOLFluiD. More details on the numerical method and physical models available in PLATO may be found in [22]. The reference chemical model for the Martian atmosphere is the 18-species 33-reactions model proposed by [23]. As the maximum entry velocity of ExoMars Schiaparelli is below 5.9 km/s, a reduced mechanism is considered. This reduced mechanism, which is accurate enough to simulate the electron density for the conditions adopted here, is a 14-species mixture made of CO_2, CO, CO^+ NO,

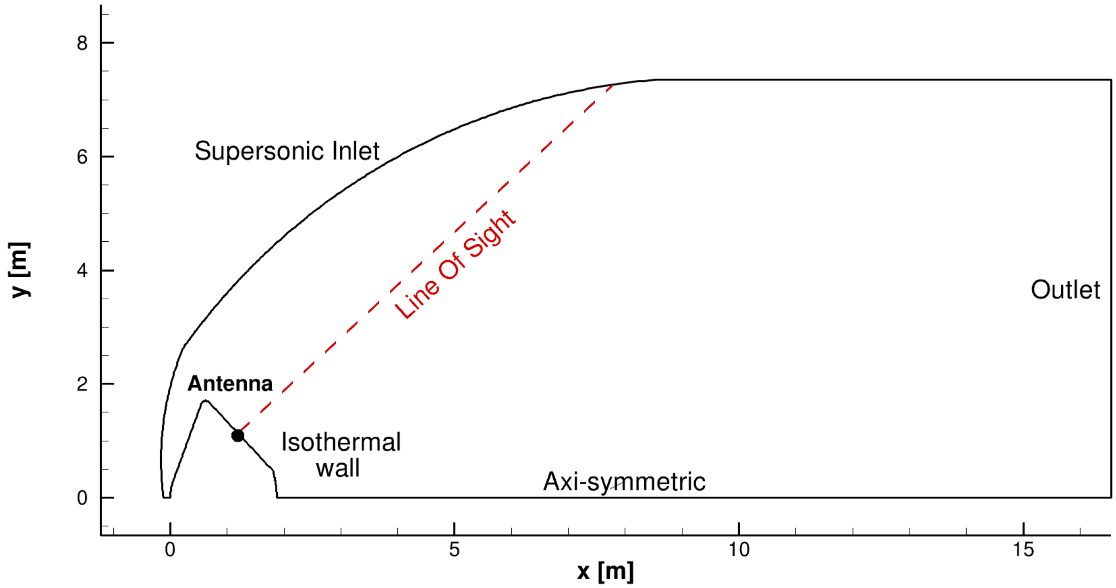

Figure 2: Computational domain with boundary conditions and antenna location.

Case	$t[s]$	$h[km]$	ρ_∞ $[kg/m^3]$	V_∞ $[m/s]$	T_∞ $[K]$	M_∞
a	38	80	3.72 e-05	5856	175	27.5
b	80	52	8.25 e-04	3941	180	18.2
c	92	48	1.27 e-03	3006	189	13.6

Table 1: Free stream conditions of ExoMars Schiaparelli at different trajectory points.

NO^+, N_2, O_2, O_2^+ , N, C, C^+, O, O^+, e, adapted from [23], where it was also shown that, for the velocity regime of this work, a single temperature could be used to account for non-equilibrium effects.

Figure 2 shows the computational domain used in this study. The ExoMars Schiaparelli geometry is a 71 degree sphere cone front shield with a nose radius of 0.06 m and an overall vehicle diameter of 2.4 m. A 0.06 m radius shoulder connects the forebody to a 47-deg conical back shield. ANSYS ICEM CFD Release 20.1® has been used to create a multiblock grid, which has been gradually coarsened towards the wake region and is orthogonal to the body at its surface. The computational domain extends 10 vehicles radii downstream to allow for an extended representation of the wake. To reduce the computational cost, the flow is assumed axi-symmetric which can be considered a valid assumption as the maximum angle of attack during entry is 6 degrees over the entire trajectory. The free-stream conditions for the trajectory points investigated here are given in table 1. The flow-field is further assumed to be steady and laminar, with a free-stream composition of 96% CO_2 and 4% N_2. The vehicle walls are assumed non-catalytic and iso-thermal, with temperature set to 1500 K.

3.2 Optical plasma properties

The flow field solution obtained from the hypersonic CFD simulations contain the information on the plasma, that are used as input for the ray tracing analysis. Ray tracing allows for analysing the propagation of EM waves on the basis on the computation of the optical properties of the plasma, which are defined by the refractive index. The optical properties are described by the Appleton-Hartree equation, which has been extensively applied to ionospheric propagation problems [24]. The entry plasma is modeled as an unmagnetised cold plasma, a common assumption for atmospheric entry flows. Under these assumptions, the Appleton-Hartree equation reads:

$$n^2 = (\mu - \imath\chi)^2 = 1 - \frac{X}{1 - \imath Z}, \tag{1}$$

with:

$$\begin{aligned} X &= \mathrm{e}^2 N_\mathrm{e} / \left(\epsilon_0 m_\mathrm{e} \omega^2\right), \\ Z &= \nu_\mathrm{eh}/\omega, \\ \omega &= 2\pi f, \end{aligned} \tag{2}$$

where e denotes the electron charge, N_e the electron number density, ϵ_0 the vacuum permittivity, m_e the electron mass, ν_eh the electron-heavy particle collision frequency, and f for the communication system transmission frequency.

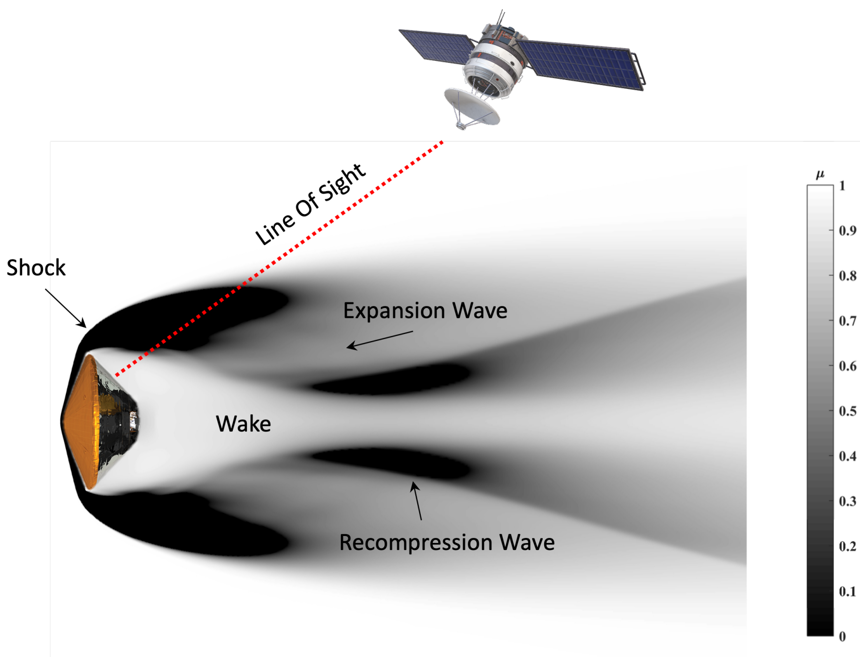

Figure 3: Wake flow structure with refractive index μ over re-entry capsule

The plasma complex refractive index, n, consist of a real part, μ, and an imaginary part, χ. The real part represents the effects of EM waves bending, whereas the imaginary part is related to the absorptivity and is responsible for EM wave attenuation. The effect of neglecting or considering electron collisions in the Appleton-Hartree equation can lead to two different medium characterizations, non-collisional and collisional plasma. Usually the electron plasma frequency is large compared to the electron - heavy particle collision frequency. As reported in [13], for CO_2 atmospheric entry the simplification of non-collisional medium is a good approximation to describe plasma characteristics generated by the ionisation level occuring in the entry conditions of the ExoMars capsule. For non-collisional plasma, $Z \sim 0$, meaning $\nu_{eh} \ll \omega$, leading to:

$$n = \mu = \sqrt{1 - X} = \sqrt{1 - \left(\frac{f_p}{f}\right)^2}, \tag{3}$$

with:

$$f_p = \sqrt{kN_e} \tag{4}$$

$$k = e^2 / \left(4\pi^2 \epsilon_0 m_e\right) \tag{5}$$

In this formulation, the refractive index is a real number with values between 0 and 1. The refractive index of the plasma thus becomes a solely a function of the electron plasma frequency f_p and the antenna transmission frequency ω in Hz. Figure 3 describes the distinctive flow structure within the wake flow of a re-entry capsule and its refractive index field. The front part of the flow is characterized by the presence of an hypersonic thin shock layer, which produce flow ionization. This zone presents the highest values of electron densities, making communications impossible in this direction, with an overall refractive index equal to 0 in the whole front shock layer. The flow is then turned around the shoulder of the vehicle resulting in an expansion fan, which curves the bow shock, decrease the temperature and accelerates the flow. In this region, due to lower temperature values, recombination occurs, reducing the presence of free electrons, as visible from higher values of the refractive index. The expansion region is followed by a recompression shock, that is created as the flow realigns in the wake. The occurrence of different flow features significantly changes the optical properties of the gas, leading to refractive index around unity in colder regions, and to refractive index approaching zero values where ionization levels are higher.

3.3 3D Ray tracing algorithm

To compute the EM waves propagation through the entry plasma, this work makes use of a ray tracing algorithm based on the Eikonal equation. The Eikonal equation is an approximate solution of Maxwell's equations in the high-frequency limit [25]. At large frequencies, electric and magnetic fields may be expressed as:

$$\begin{aligned} E(r) &\simeq E_0 e^{-\imath k_0 S(r)} \\ H(r) &\simeq H_0 e^{-\imath k_0 S(r)}, \end{aligned} \tag{6}$$

where $S(r)$ is the normalised Eikonal phase function, defining the wave-front surface. Inserting the high frequency fields into Maxwell's equations leads to the Eikonal equation:

$$|\nabla S| = \mu, \tag{7}$$

that defines the relation between the direction of propagation of an EM wave and the refractive index of the medium. The equation 7 can be rewritten in characteristic form, with the advantage of a more convenient representation to retrieve ray trajectories equations. This may be achieved by introducing the normalized local wave vector$\xi = \nabla S$K, that defines the propagation direction of the EM wave, and the position vector $x_i = (x_1, x_2)$. Using the arc-length s along the ray, one arrives at the following system of ordinary differential equations:

$$\begin{aligned} \frac{\partial x_i}{\partial s} &= \frac{\xi_i}{\mu}, \\ \frac{\partial \xi_i}{\partial s} &= \frac{\partial \mu}{\partial x_i}. \end{aligned} \tag{8}$$

The Eikonal approximation is valid as long as medium properties vary slowly over a length-scale of the order of the signal wavelength [25]. In an hypersonic entry plasma, this assumption can be considered valid in the whole wake region. As visible in 3 strong gradients are mainly located in the front part of the vehicle, a zone non suitable for the propagation of EM waves due to the high ionisation level of the flow. The system 8, along with prescribed initial conditions in terms of position and angle of the emitted ray, allows to predict ray trajectories and states that the curvature of rays at each point is proportional to the gradient of the refractive index. For three-dimensional space, the ray trajectories system of equations 8 reads as follow:

$$
\begin{aligned}
\frac{\partial x}{\partial s} &= \frac{\xi_1}{n}, \qquad & \frac{\partial \xi_1}{\partial s} &= \frac{\partial n}{\partial x} \\
\frac{\partial y}{\partial s} &= \frac{\xi_2}{n}, \qquad & \frac{\partial \xi_2}{\partial s} &= \frac{\partial n}{\partial y} \\
\frac{\partial z}{\partial s} &= \frac{\xi_3}{n}, \qquad & \frac{\partial \xi_3}{\partial s} &= \frac{\partial n}{\partial z}
\end{aligned} \tag{9}
$$

In this work the 3D ray trajectories are computed using an updated version of BORAT, a MATLAB® code developed for the plasma modeling and ray tracing integration. The Ordinary Differential Equations (ODE) system resulted from the Eikonal equation (9) is solved in each step using a Runge-Kutta method (RK4). For a given ray, initial conditions are prescribed in terms of position and angle:

$$
\begin{aligned}
x(s)|_{s=0} &= x_0, \qquad & \xi_1(s)|_{s=0} &= cos(\theta_0)cos(\alpha_0) \\
y(s)|_{s=0} &= y_0, \qquad & \xi_2(s)|_{s=0} &= cos(\theta_0)sin(\alpha_0) \\
z(s)|_{s=0} &= z_0, \qquad & \xi_3(s)|_{s=0} &= sin(\theta_0)
\end{aligned} \tag{10}
$$

where the angle α_0 is the angle on the plane x-y, and the angle θ_0 is the azimuthal angle respect the positive z axis. Rays integration is completed when either they emerge from the computational domain or if the ray impinges the vehicle surface. The vehicle outer surface is modelled as a metallic solid wall, assuming that the presence of heat shields materials does not affect the refractive property of the body. Thus, a solid reflection boundary condition is imposed when a ray impinges on the vehicle surface. In this case, new initial conditions are imposed to the ray, that will be reshoot from the intersection point. In conclusion, the proposed ray tracing method results in a numerically efficient tool. Each ray is independent and uncoupled respect the other rays, and the solver can be easily parallelized with complexity scale that varies linearly with the number of rays. Figure 4 summarize the numerical methodology to analyze communication blackout used in this work.

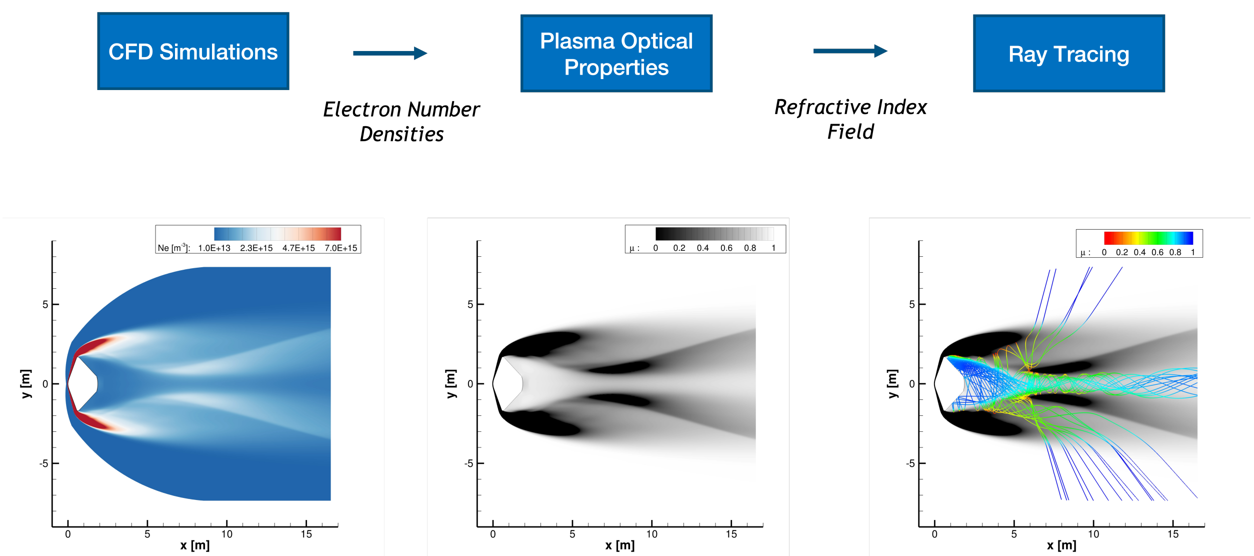

Figure 4: Radio frequency blackout analysis methodology: from CFD simulations to ray tracing analysis.

4 Results

In this section the flow-field solution at the three different trajectory points are shown. The first step has been the duplication of the solution respect the symmetry axis in order to set-up a full bi-dimensional analysis of the blackout phenomena. Figures 5 and 6 show the different temperature and electron number density fields at 38, 80 and 92 seconds during the re-entry trajectory, with respectively a free-stream Mach number of 27, 18 and 13.

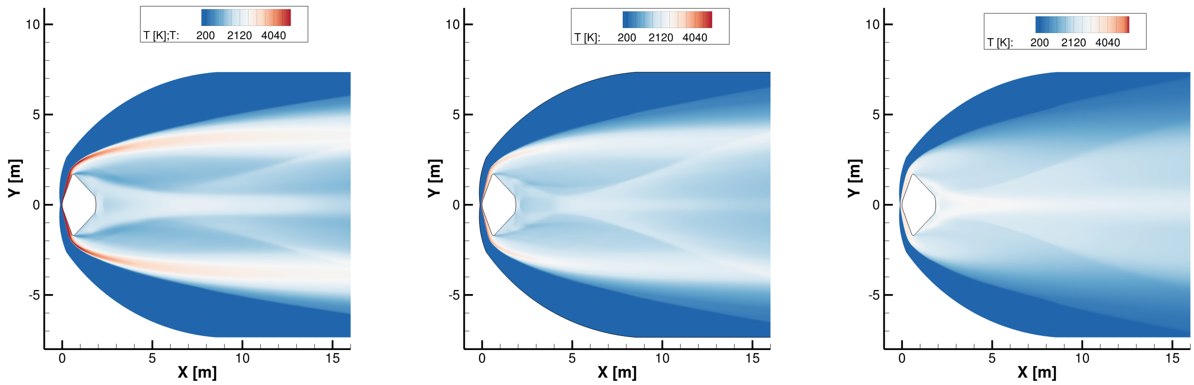

Figure 5: Temperature fields: 38s (left), 80s (center), 92s (right).

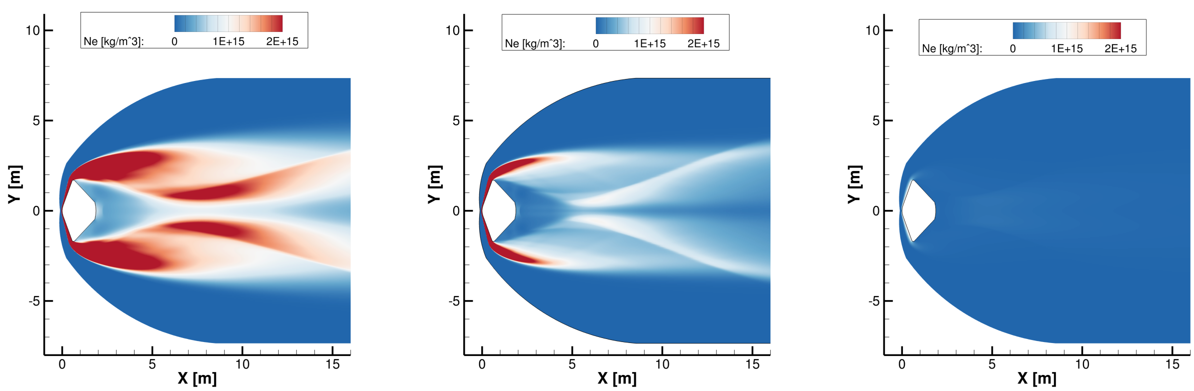

Figure 6: Electron Number Density N_e fields: 38s (left), 80s (center), 92s (right).

The main flow feature that characterize the solutions is the strong shock generated in front of the spacecraft that allows the flow to decelerate and pass over the surface of the body. In this region high temperature peaks arise and the ionization levels of the flow reach their maximum. Subsequently, the flow is cooled down and accelerated over the vehicle shoulder by an expansion fan, that lowers the ionization levels of the flow. Generally, this is the region where spacecrafts mount communications antennas to partially overcome blackout conditions during the re-entry. The wake region is characterized by a recirculation region and a recompression zone, that highers electron densities in the wake. The refractive index, the parameter describing the propagation of an EM wave in plasma, is computed and displayed for the selected ExoMars trajectory points in figure 7 for the ExoMars on-board antenna transmission frequency of $f = 400$Mhz. At 38s after the entry in the martian atmosphere, the high velocity of the vehicle generates high temperature effects that leads to an high ionization of the flow. In all cases the refractive index approaches unity in the free-stream zones, at the side edges of the shock wave and in the central part of the wake. The 92s solution

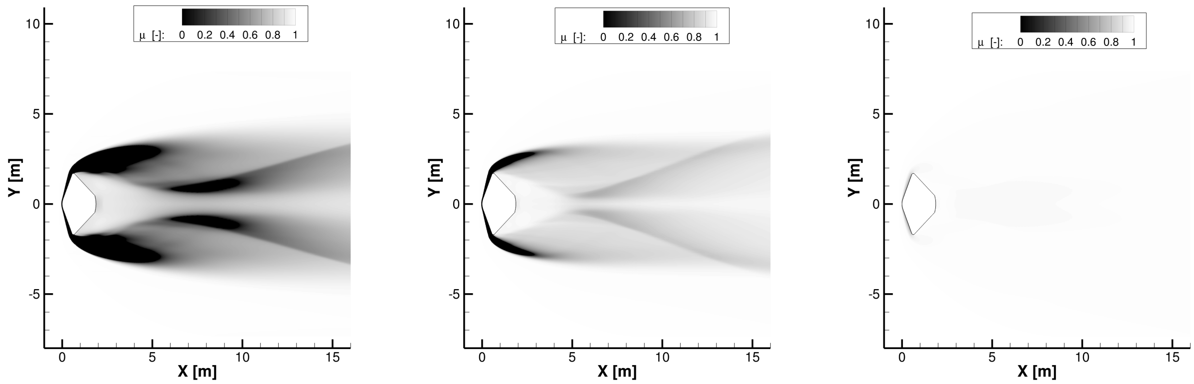

Figure 7: Refractive index μ fields: 38s (left), 80s (center), 92s (right).

point belong to the terminal phase of the blackout period of the ExoMars capsule. Ionisation levels are low respect the critical electron number density of the emitting antenna frequency, thus the refractive index field is almost equal to 1 in the whole domain.

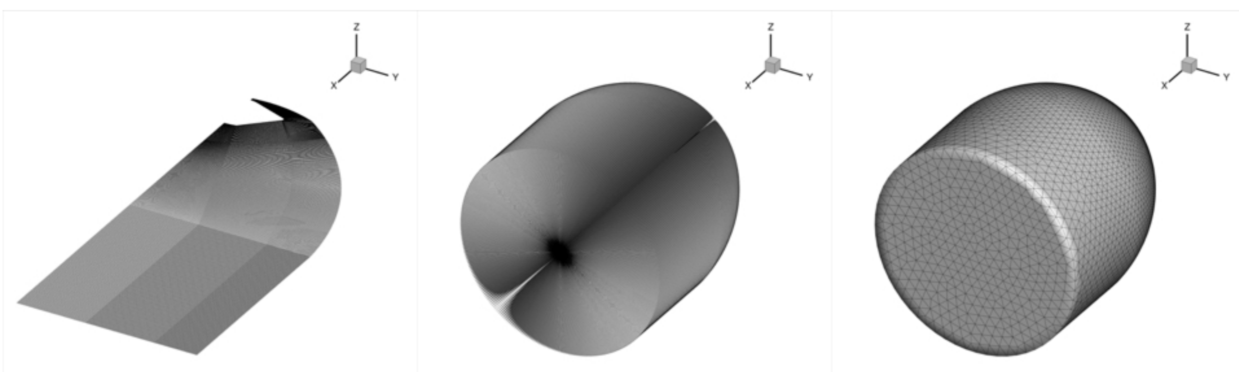

Figure 8: ExoMars solution reconstruction with 3D interpolation from 2D axisymmetric solution.

Once the optical properties of the flow are computed, the next step is the generation of a three-dimensional solution to perform ray tracing integration. Due to the low angle of attack flight conditions of the ExoMars amtospheric entry phase, in first approximation the 2D axisymmetric solution can be considered representative of the a fully 3D CFD computation. To generate a three-dimensional CFD solution input for the ray tracing solver, the bi-dimensional solutions have been reconstructed on a three-dimensional mesh. Figure 8 shows the intermediate steps of this procedure. The 3D reconstructed solution is based on 6 million cells unstructured tetrahedral mesh, generated with the mesh generation software Gambit. The 2D structured solution is interpolated on the 3D mesh via an inverse distance interpolation algorithm.

After the generation of the 3D input solution files via interpolation, the ray tracing analysis has been carried on for all the re-entry trajectory point listed in Table 1. For the three-dimensional analysis, the emitting antenna is located on the vertical side of the spacecraft, and the emitted signal is modelled with an omnidirectional beam of 180 rays with a 70 degrees cone aperture respect the normal to the spacecraft. As shown in 9, for each solution two different iso-surfaces are highlighted: the first iso-surface (darker in colour and close to the spacecraft body) is the μ=0 surface, that delimits the zones at high ionisation generated during the blackout and shields the emitted signal from the propagation in the plasma layer. The iso-surface at $\mu = 1$ delimits the bow shock surface, from which the plasma layer is generated around the spacecraft.

Figures 10-12 show the 3D ray tracing solutions. For each solution two different iso-surfaces are highlighted: the first iso-surface (darker in colour and close to the spacecraft body) is the $\mu = 0$ surface, that delimits the zones at high ionisation generated during the blackout and shields the emitted signal from the propagation in the plasma layer. As predicted, its extension varies during the re-entry, with its peak at the trajectory points 38s, in which the flight conditions are of complete blackout. On the other hand, the iso-surface at $\mu = 1$ delimits the bow shock surface, from which the plasma layer is generated around the spacecraft. Its extension depends on the Mach number of the flow, and decreases during the re-entry decel-

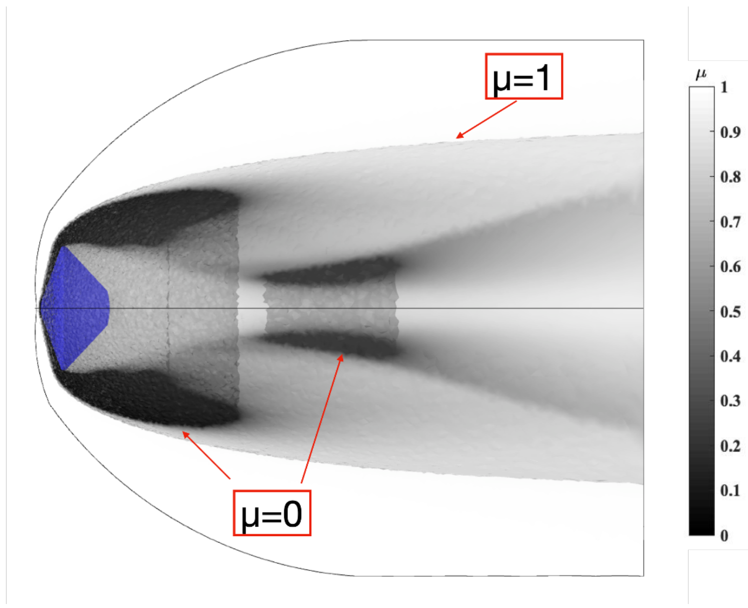

Figure 9: Iso-surfaces definition for 3D ray tracing visualization: x-y plane view.

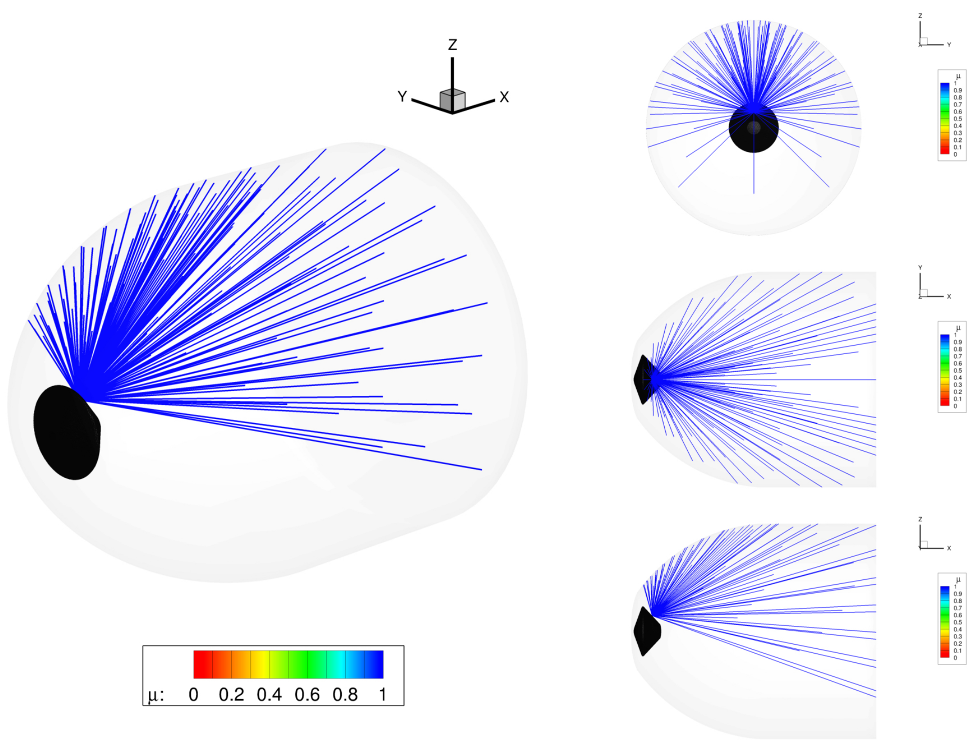

Figure 10: 3D ExoMars ray tracing solution at 92s re-entry trajectory point

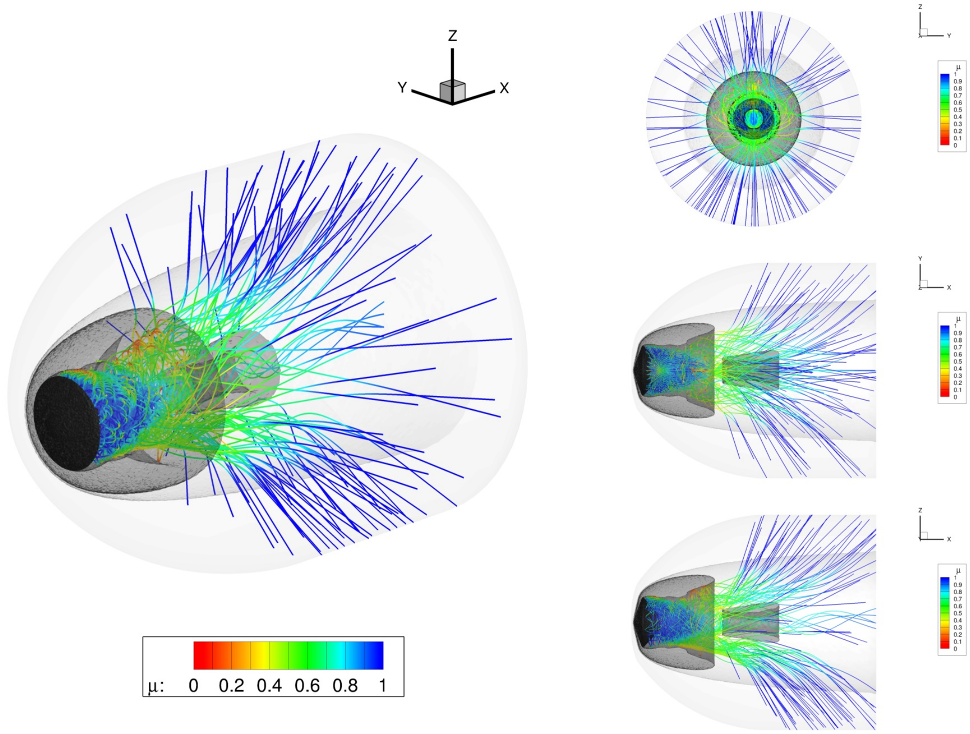

Figure 11: 3D ExoMars ray tracing solution at 38s re-entry trajectory points

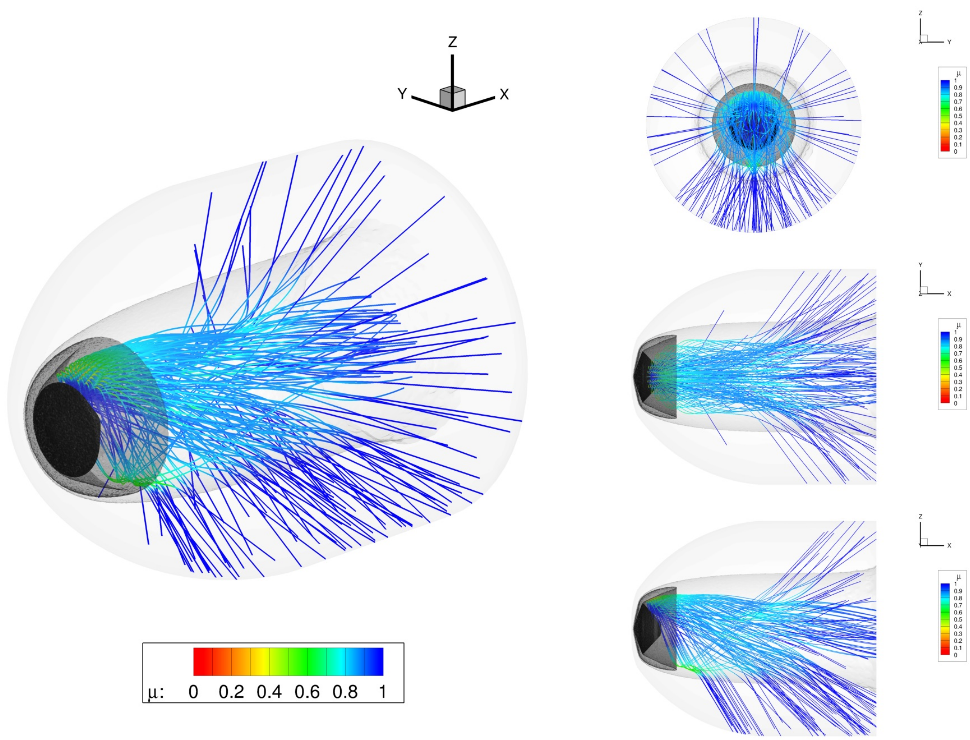

Figure 12: 3D ExoMars ray tracing solution at 80s re-entry trajectory points

eration phase. All rays are coloured depending on the refractive index value of the field encountered in their path. Rays encounter strong reflections near the shoulder of the vehicle and a series of refractions in the wake region. At maximum blackout conditions, the vast majority of the rays are converged in the wake and shielded by the plasma. Brownout phases are characterized by lower ionisation levels of the flow that result in less disruption of the electromagnetic wave signal, as visible in the trajectory point at 80s. In general, the entry plasma wraps the vehicle and forms a shielding cup around it. Because of the reflection at the plasma, the cup has a potential for focussing/defocussing the rays, a fact that may generate directive patterns in certain angular regions. During brownout, not all the electromagnetic waves are fully encapsulated in the plasma layer. In this condition, the presence of plasma redirects the rays, creating communication windows that could possibly be used as alternative communication path. Future works will be focused on the investigation of alternative communication windows.

In conclusion, at the onset and end of the blackout phase it is not likely that all EM waves are fully contained within the plasma layer. Reflections and refractions of the emitted EM waves are the leading phenomena of these re-entry phases, and their effect must be taken into account. The use of ray tracing allows to gather information on possible alternative communication directions during these flight phases, since the accurate EM waves path can be fully reproduced with this method. This analysis is extremely important for both characterizing accurately enough the blackout physical phenomena and to gather important information for possible mitigation solutions.

5 Conclusion

This work presents the application of a ray tracing method for the blackout analysis of the ExoMars Schiaparelli mission. The proposed methodology, based on research efforts carried on at the von Karman Institute for Fluid Mechanics over the past years, has been applied to the Martian re-entry of the ExoMars Schiaparelli module in [12] and [13] with a two-dimensional approach. In this work, the blackout numerical solver is upgraded to a three-dimensional formulation to deliver a tool capable of reproducing real flight configurations. It is based on the application of CFD simulations, performed with the COOLFLuiD aerothermodynamic solver and the PLATO library for non-equilibrium plasmas, in combination with the 3D ray tracing solver BORAT. Numerical CFD simulation are performed at different entry trajectory points assuming chemical non-equilibrium and thermal equilibrium for a 14 species Martian atmosphere mixture. Results confirm that radio blackout is mostly due to encapsulation of rays by the plasma rather than absorption of the signal. Furthermore, reflection and refraction phenomena can make RF signal rays escape the entry plasma layer. Advanced analysis methods, such as the one presented in this work, allows for properly predicting the emitted signal path in the plasma flow, thus gathering more information on possible alternative communication directions during blackout. This is extremely important for the brownout phases, where, due to lower ionization levels of the flow, the emitted radio waves can possibly reach the receiving spacecraft through refraction and reflection.

Acknowledgments

The research of Vincent Fitzgerald Giangaspero is supported by SB PhD fellowship 1SA8219N of the the Research Foundation - Flanders (FWO).

The resources and services used in this work were provided by the VSC (Flemish Supercomputer Center), funded by the Research Foundation - Flanders (FWO) and the Flemish Government.

References

[1] Yusuke Takahashi, Taiki Koike, Nobuyuki Oshima, and Kazuhiko Yamada. Aerothermodynamic analysis for deformed membrane of inflatable aeroshell in orbital reentry mission. *Aerospace Science and Technology*, 92:858–868, 2019.

[2] K. Minkwan, M. Keidar, and I. D. Boyd. Analysis of an electromagnetic mitigation scheme for reentry telemetry through plasma. *Journal of Spacecraft and Rockets*, 45(6):1223–1229, 2008.

[3] S. Portigliotti, C. Cassi, M. Montagna, P. Martella, M. Faletra, J. Boi, S. De Sanctis, D. Granà, O. Bayle, T. Blancquaert, et al. Exomars 2016, the schiaparelli mission. edl demonstration results from real time telemetry before unfortunate impact. In *14th International Planetary Probe Workshop*, 2017.

[4] Toni Tolker-Nielsen. Exomars 2016-schiaparelli anomaly inquiry. 2017.

[5] Antonio Viviani, Andrea Aprovitola, Luigi Iuspa, and Giuseppe Pezzella. Aeroshape design of reusable re-entry vehicles by multidisciplinary optimization and computational fluid dynamics. *Aerospace Science and Technology*, 105:106029, 2020.

[6] Minkwan Kim. Active plasma layer manipulation scheme during hypersonic flight. *Aerospace Science and Technology*, 35:135–142, 2014.

[7] Iain Boyd. Modeling of plasma formation in rarefied hypersonic entry flows. In *45th AIAA Aerospace Sciences Meeting and Exhibit*, page 206, 2007.

[8] D. Morabito, R. Kornfeld, K. Bruvold, L. Craig, and K. Edquist. The mars phoenix communications brownout during entry into the martian atmosphere. *The Interplanetary Network Progress Report*, 42:179, 2009.

[9] Hui Zhou, Xiaoping Li, Kai Xie, Yanming Liu, and Yuanyuan Yu. Mitigating reentry radio blackout by using a traveling magnetic field. *Aip Advances*, 7(10):105314, 2017.

[10] DD Morabito. The spacecraft communications blackout problem encountered during passage or entry of planetary atmospheres. *IPN Progress Report*, pages 42–150, 2002.

[11] D. Morabito, B. Schratz, K. Bruvold, P. Ilott, K. Edquist, and A. D. Cianciolo. The mars science laboratory edl communications brownout and blackout at uhf. *Interplanetary Network Progress Report*, 197(27):1–22, 2014.

[12] S. Ramjatan, A. Lani, S. Boccelli, B. Van Hove, Ö Karatekin, T. Magin, and J. Thoemel. Blackout analysis of mars entry missions. *Journal of Fluid Mechanics*, 904, 2020.

[13] Vincent F Giangaspero, Andrea Lani, Stefaan Poedts, Jan Thoemel, and Alessandro Munafò. Radio communication blackout analysis of exomars re-entry mission using raytracing method. In *AIAA Scitech 2021 Forum*, page 0154, 2021.

[14] Y. Takahashi, R. Nakasato, and N. Oshima. Analysis of radio frequency blackout for a blunt-body capsule in atmospheric reentry missions. *Aerospace*, 3(1):2, 2016.

[15] A. Lani, T. Quintino, D. Kimpe, H. Deconinck, S. Vandewalle, and S. Poedts. The coolfluid framework: design solutions for high performance object oriented scientific computing software. In *International Conference on Computational Science*, pages 279–286. Springer, 2005.

[16] Andrea Lani. An object oriented and high performance platform for aerothermodynamics simulation. *Université Libre de Bruxelles*, 2008.

[17] M. Panesi, A. Lani, T. Magin, J. Molnar, O. Chazot, and H. Deconinck. Numerical investigation of the non equilibrium shock-layer around the expert vehicle. In *18th AIAA Computational Fluid Dynamics Conference*, page 4317, 2007.

[18] D. Knight, O. Chazot, J. Austin, M.A. Badr, G. Candler, B. Celik, D. De Rosa, R. Donelli, J. Komives, A. Lani, et al. Assessment of predictive capabilities for aerodynamic heating in hypersonic flow. *Progress in Aerospace Sciences*, 90:39–53, 2017.

[19] M-S. Liou. A sequel to ausm: Ausm+. *Journal of computational Physics*, 129(2):364–382, 1996.

[20] T.J. Barth. Aspects of unstructured grids and finite-volume solvers for the euler and navier-stokes equations. *AGARD, Special Course on Unstructured Grid Methods for Advection Dominated Flows*, 1992.

[21] V. Venkatakrishnan. On the accuracy of limiters and convergence to steady state solutions. In *31st Aerospace Sciences Meeting*, page 880, 1993.

[22] A. Munafò, A. Alberti, C. Pantano, and M. Freund, J.B. Panesi. A computational model for nanosecond pulse laser-plasma interactions. *J. Comput. Phys.*, 406:109190, 2020.

[23] C. Park, J.T. Howe, R.L. Jaffe, and G.V. Candler. Review of chemical-kinetic problems of future nasa missions. ii-mars entries. *Journal of Thermophysics and Heat transfer*, 8(1):9–23, 1994.

[24] K. Davies. *Ionospheric radio propagation*, volume 80. US Department of Commerce, National Bureau of Standards, 1965.

[25] Yury A Kravtsov and Yuri Ilich Orlov. *Geometrical optics of inhomogeneous media*, volume 38. Springer, 1990.